

# DEVELOPMENT OF A PLANETARY ENTRY SYSTEMS SYNTHESIS TOOL FOR CONCEPTUAL DESIGN AND ANALYSIS

D.M. Kipp<sup>(1)</sup>, J.A. Dec<sup>(2)</sup>, G.W. Wells<sup>(3)</sup>, R.D. Braun<sup>(4)</sup>

*Space Systems Design Lab, Georgia Institute of Technology, 270 Ferst Drive, Atlanta, GA 30332, USA*

<sup>(1)</sup>Email: [devin\\_kipp@ae.gatech.edu](mailto:devin_kipp@ae.gatech.edu)

<sup>(2)</sup>Email: [John.A.Dec@nasa.gov](mailto:John.A.Dec@nasa.gov)

<sup>(3)</sup>Email: [gfg315z@mail.gatech.edu](mailto:gfg315z@mail.gatech.edu)

<sup>(4)</sup>Email: [rbraun@mail.ae.gatech.edu](mailto:rbraun@mail.ae.gatech.edu)

## ABSTRACT

A Planetary Entry Systems Synthesis Tool, with applications to conceptual design and modeling of entry systems has been developed. This tool is applicable to exploration missions that employ entry, descent and landing or aerocapture. An integrated framework brings together relevant disciplinary analyses and enables rapid design and analysis of the atmospheric entry mission segment. Tool performance has been validated against Mars Pathfinder flight experience and has direct relevance to future NASA robotic and human space exploration systems.

## 1. INTRODUCTION

The Planetary Entry Systems Synthesis Tool (PESST) has been developed within the Space Systems Design Laboratory at the Georgia Institute of Technology to enable rapid design and analysis of systems for entry, descent and landing (EDL) and aerocapture. The tool integrates relevant disciplinary analyses including aeroshell geometry, atmospheric modeling, vehicle aerodynamics, atmospheric flight mechanics, aerothermodynamics, and thermal analysis within a single multidisciplinary design framework. The tool is intended for application to conceptual design and analysis. Theory and implementation are discussed in this paper, along with validation against Mars Pathfinder flight experience.

## 2. AEROSHELL GEOMETRY

A review of aeroshell geometries used in previous planetary entry missions was completed to determine what basic shapes should be modeled in PESST. It was determined that four simple geometries, depicted in Figure 1, should be explicitly

represented: sphere-cones, biconics, capsules, and probes. While the sphere-cones and probes have identical forebody geometries, the probe design has a spherical aftbody compared to the flat aftbody of a nominal sphere-cone.

Each shape requires a unique set of inputs to fully define its geometry as illustrated in Figure 2. Key parameters such as aerodynamic reference area, surface area, wetted area, length, and volume are determined from these inputs. In addition, a three dimensional triangular surface mesh of the body is generated. This surface mesh is necessary for calculation of aerodynamic coefficients and also enables visualization of the aeroshell geometry.

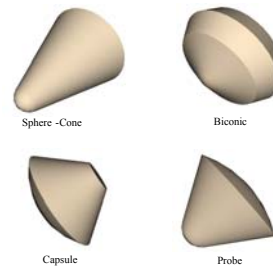


Fig. 1. Basic Aeroshell Geometries

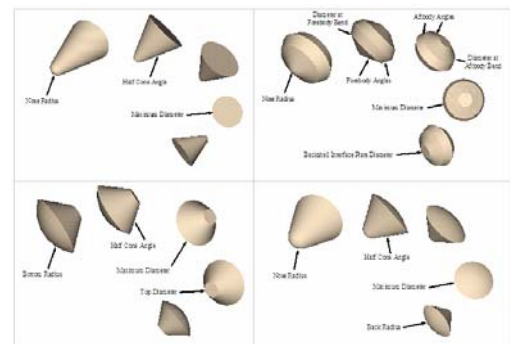


Fig. 2. Geometric Input Parameters

Aeroshell body axes are defined so the x-axis is aligned with the centerline of the body. The

surface radius at points along the x-axis is then calculated. Since each shape is axis-symmetric, a circle of this radius contains all the points on the surface of the shape at this axial location along the centerline. In this manner, a grid of nodes is defined over the entire surface and the nodes are connected to discretize the surface into triangles. This process is illustrated in Figure 3.

An output file, containing the vertices and outward normal vector for each triangle, is generated to store the surface mesh. This output file is read directly by the aerodynamics module to compute aerodynamic coefficients. In addition, this file is used to generate a navigable VRML file for full visualization of the generated geometry.

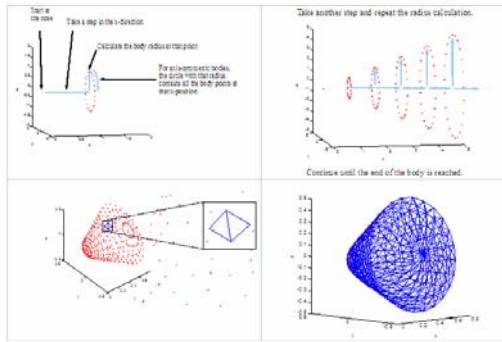


Fig. 3. Surface Mesh Generation

As an alternative to using the pre-defined shapes, a NASTRAN file may be used to import the geometry of any user-defined vehicle. This allows custom geometries, modeled within CAD programs, to be imported into PESST. For this input option, geometric characteristics such as aerodynamic reference area must be entered directly.

### 3. HYPERSONIC AERODYNAMICS

Modified Newtonian aerodynamics [1] are a simple and accurate method for determining aerodynamic coefficients of the entry body during continuum hypersonic flow – the region of most interest during planetary entry and aerocapture missions due to the high aerodynamic heating and deceleration. In Newtonian aerodynamic theory, local pressure coefficient is solely a function of vehicle geometry, which PESST has computed in the form of a triangular surface mesh. For each panel, the pressure coefficient is given by modified Newtonian theory as:

$$C_p = C_{p_{\max}} \sin^2 \delta \quad (1)$$

Where  $C_{p_{\max}}$  is the stagnation point pressure coefficient, which can be approximated as constant for a given atmosphere, and  $\delta$  is the local angle between the incoming velocity vector and the geometric body. This angle is determined from the incoming velocity vector and the local surface normal according to:

$$\delta = \frac{\pi}{2} - \cos^{-1} \left( \frac{\vec{n} \cdot \vec{V}}{|\vec{n}| |\vec{V}|} \right) \quad (2)$$

The velocity vector can be represented in terms of angle of attack,  $\alpha$ , and sideslip angle,  $\beta$ , according to:

$$\vec{V} = V_{\infty} \cos \alpha \cos \beta \quad -V_{\infty} \sin \beta \quad V_{\infty} \sin \alpha \cos \beta \quad (3)$$

In this manner the pressure coefficient is calculated for each triangular panel represented in the surface mesh. Breaking the coefficients for each panel into their representative body axis components,  $C_x, C_y, C_z$ , enables us to determine the overall forces in the body axis by summation:

$$C_x = \frac{1}{S_{ref}} \sum_i C_{xi} S_i \quad (4)$$

where individual panel areas,  $S_i$ , are determined from the triangle's vertices by first calculating the length of each side and then applying Heron's formula. The summation is then normalized by the aerodynamic reference area,  $S_{ref}$ , to maintain units of force. Finally, aerodynamic lift and drag coefficients,  $C_L$  and  $C_D$ , are calculated according to:

$$C_L = -C_x \sin \alpha + C_z \cos \alpha \quad (5)$$

$$C_D = C_x \cos \alpha \cos \beta - C_y \sin \beta + C_z \sin \alpha \cos \beta \quad (6)$$

This method generates aerodynamic coefficients for input angles of attack and sideslip. Repeating this process at varying angles of attack allows population of lift and drag coefficient tables as functions of angle of attack. These tables are necessary to propagate the atmospheric trajectory.

## 4. ATMOSPHERE FLIGHT MECHANICS

Simulation of atmospheric flight within PESST is performed using a three degree-of-freedom trajectory analysis specially developed for this application [12]. This trajectory analysis is capable of simulating both ballistic and lifting entry trajectories at arbitrary planetary bodies. A modest guidance capability is included that enables modeling of aerocapture and guided entry simulations. Event modeling capabilities include vehicle staging, parachute inflation, parachute release, and terminal propulsive descent based on a gravity turn control law.

### 4.1 Atmosphere and Gravity Models

A spherical planet model is used to approximate the target body. The gravity model is specified by the surface radius ( $r_0$ ) and gravitational parameter ( $\mu$ ) of the target body, from which the force of gravity at the surface ( $g_0$ ) is determined. Local gravitational acceleration is determined throughout the trajectory as a function of planetocentric altitude ( $h$ ) according to an inverse square gravity model:

$$g = g_0 \left( \frac{r_0}{r_0 + h} \right)^2 \quad (7)$$

The atmosphere of the target planet is modeled according to an exponential atmosphere model or through tabular data input. An exponential model is specified by the surface density ( $\rho_0$ ) and atmospheric scale height ( $H$ ) of the target planet. Local atmospheric density is then determined throughout the trajectory as a function of altitude according to:

$$\rho = \rho_0 e^{\left(\frac{-h}{H}\right)} \quad (8)$$

Local atmospheric temperature is not modeled within the tool. Instead, to determine the local Mach number of the entry vehicle, a reference speed of sound ( $a_0$ ) is included as an input. Atmospheric speed of sound does not vary significantly with altitude, so approximating the local Mach number from  $a_0$  is a reasonable approximation. If higher accuracy is desired, the speed of sound can be input in tabular form as a function of altitude.

For many entry problems planetary rotation rate ( $\omega$ ) can impact the trajectory significantly, and is included as an additional input. The

complete planetary model is specified by six key variables;  $r_0$ ,  $\mu$ ,  $\rho_0$ ,  $H$ ,  $a_0$ , and  $\omega$ .

### 4.2 Trajectory Propagation

The 3-DOF planetary entry trajectory is determined by integrating the equations of motion. Assuming a constant mass, non-thrusting vehicle, the 3-DOF point mass atmospheric flight mechanics of the entry vehicle over a spherical rotating planet are governed by the following equations of motion [2]:

$$\dot{\theta} = \frac{\cos(\gamma)\cos(\phi)}{r \cos(\phi)} * V \quad (9)$$

$$\dot{\phi} = \frac{\cos(\gamma)\sin(\phi)}{r} * V \quad (10)$$

$$\dot{r} = -\sin(\gamma) * V \quad (11)$$

$$\dot{\psi} = -\frac{\cos(\gamma)\cos(\phi)\tan(\phi)}{r} * V + \frac{L\cos(\gamma)\sin(\sigma)}{V} + \dot{\psi}_\omega \quad (12)$$

$$\dot{\gamma} = \left( g - \frac{V^2}{r} \right) * \frac{\cos(\gamma)}{V} - \frac{L\cos(\sigma)}{V} + \dot{\gamma}_\omega \quad (13)$$

$$\dot{V} = -D + g \sin(\gamma) + \dot{V}_\omega \quad (14)$$

The first three equations are the kinematic equations, which yield time derivatives of longitude ( $\theta$ ), latitude ( $\phi$ ), and radial distance to the planet center ( $r$ ) respectively. The latter three equations are the force equations, which yield time derivatives of azimuth ( $\psi$ ), flight path angle ( $\gamma$ ), and velocity ( $V$ ) respectively. Other terms are lift ( $L$ ) and drag ( $D$ ) specific forces, gravity ( $g$ ), and vehicle bank angle ( $\sigma$ ).

Terms denoted with an  $\omega$  subscript are effects due to planetary rotation. In general the rotation rate of a planet is small and these effects are negligible. However, for long-range high-speed flight (e.g. shuttle entry) or large radius bodies (e.g. Jupiter) the effect becomes significant.

### 4.3 Event Modeling

Many different event types may be encountered during a typical planetary entry. These include parachute deployment, parachute release, vehicle staging, and descent propulsion events. The events can occur separately or overlap (e.g. heatshield

separation while on parachute). Each of these event types is triggered by any of several variables including: dynamic pressure, Mach number, altitude, density, deceleration, velocity, and various timer options. An event begins when the designated variable passes through a preset 'trigger value' with either increasing or decreasing slope according to the chosen input option.

#### **4.4 Initial Conditions**

The atmospheric flight simulations are initiated with a set of user-defined conditions in a planet-centered reference frame. The initial vehicle state is specified by six variables: relative velocity, altitude, longitude, latitude, relative azimuth, and relative flight path angle. Initial vehicle parameters must also be specified which include mass, reference area, nose radius, emissivity, and aerodynamic coefficients. More detailed vehicle parameters may require specification, depending on the event being modeled.

#### **4.5 Auxiliary Calculations**

The equations of motion (9) to (14) above are numerically integrated using a specified time step to yield longitude, latitude, radial position, relative azimuth, relative flight path angle, energy, and relative velocity as functions of time. This integration requires the calculation of gravity, atmospheric density, specific lift force and specific drag force at each time step. In addition to these required variables, several auxiliary variables are calculated at each time step. Landing site relative altitude is calculated based upon an input landing site terrain elevation. Mach number is determined from relative velocity and the local sound speed. Dynamic pressure, ballistic coefficient, downrange, and acceleration are determined from standard expressions.

#### **4.6 Guidance**

The trajectory simulation is capable of guided entry and aerocapture flight-path control through bank angle modulation. The default guidance algorithm included is based on the Hybrid Predictor-corrector Aerocapture Scheme (HYPAS) for application to the Aeroassist Flight Experiment (AFE). The HYPAS algorithm derivation is outlined in [3]. For aerocapture, the algorithm consists of two phases - an entry phase that guides the vehicle toward an equilibrium glide condition and an

exit phase that guides the vehicle towards a target apoapsis altitude.

## **5. THERMAL RESPONSE and TPS**

Ablative thermal protection system sizing is done using an approximate stagnation-point sizing tool [13]. Vehicle thermal response is calculated by an approximate method that uses heat of ablation data to estimate heat shield recession during entry. This analysis is coupled to a one-dimensional finite-difference calculation that determines in-depth thermal response. The in-depth solution accounts for material decomposition, but does not account for pyrolysis gas energy absorption through the material. As inputs, the method relies on trajectory data, including relative velocity, atmospheric density, pressure, and convective heat rate as a function of time. The tool calculates radiative heating, recovery enthalpy, wall enthalpy, surface pressure, and heat transfer coefficient. Ultimately, the tool determines recession thickness, total thickness, and heat shield areal mass based on thermal response at the stagnation-point. A uniform thickness heatshield is modeled.

### **5.1 Material Property Database**

In order to simplify analysis and remove some of the complexity involved in running a thermal response calculation, a materials database was constructed for common ablative thermal protection and aeroshell substructure materials. User-defined materials can be simply added to the database without having to modify the TPS tool source code.

Stored constants for ablative materials include the decomposition kinetic constants used in the Arrhenius formulation [4] for density decomposition, the resin volume fraction, the heats of formation, thermal conductivity, specific heat, emissivity, and heat of ablation curve fit constants. The thermal conductivity, specific heat, and emissivity are input as functions of temperature in tabular format and have property entries for both the virgin and char material. The substructure material property format is similar to the ablative file format with the following exceptions. Instead of the decomposition kinetic constants, only the materials density is input, there are no entries for the resin volume fraction and heats of formation. There is only one tabular entry for the specific heat and thermal conductivity

as a function of temperature, since there is no distinction between virgin and char for a back-up material.

## 5.2 Stagnation-Point Heat Rate

Using the appropriate trajectory information, stagnation-point heat rate is calculated.

The stagnation point convective heat rate is determined according to the Sutton-Graves equation [5]:

$$\dot{q}_{conv} = k \cdot (\rho / r_n)^{0.5} \cdot V^3 \quad (15)$$

Where k is a constant based on the planetary atmosphere,  $\rho$  is the free stream density,  $r_n$  is the nose radius, and V is the relative velocity.

Stagnation-point radiative heat rate is computed using the Tauber-Sutton radiative heating correlation for Earth and Mars [6]. The Tauber-Sutton formulation is a stagnation point method and is given as:

$$\dot{q}_{rad} = C \cdot r_n^a \cdot \rho^b f(V) \quad (16)$$

Where C is a constant based on the planetary atmosphere,  $r_n$  is the nose radius,  $\rho$  is the free stream density, and  $f(V)$  is a tabulated function of velocity given in [6]. The constants a and b depend on the velocity, density, planetary atmosphere, and vehicle nose radius and are defined in [6]. Once the stagnation-point radiative heat rate is calculated, it is combined with the stagnation-point convective heat rate to determine the total stagnation-point heat rate at a particular point along the trajectory.

Stagnation-point heat load is calculated by integrating the appropriate heat rate relation over the trajectory. Total heat load is computed by adding the convective and radiative components. The radiative heating, convective heating, and total heat load are output as a function of time.

## 5.3 Approximate Heat of Ablation and Finite-Difference Calculation

There are two components to the approximate technique presented here. The first component makes use of a steady state ablation assumption and employs the heat of ablation, or  $Q^*$ , to estimate recession during entry. The second component involves calculating the in-depth temperature response to predict the

amount of material required as insulation to keep the bondline temperature below a specified limit. Calculating the in-depth temperature response is accomplished using a finite-difference formulation for the in-depth conduction through the material.

Using the heat of ablation, the recession rate at any instant in time can be calculated by equation 16. The total recession is then found by integrating the recession rate over the entire trajectory. This formulation is conservative and will generally over predict recession rate.

$$\dot{s} = \frac{\dot{Q}_{hw}}{\rho \cdot Q^*} \quad (16)$$

$\dot{s}$  = the recession rate

$\rho$  = the current material density

$Q^*$  = the heat of ablation

$\dot{Q}_{hw}$  = the hot wall heat flux

The one-dimensional heat conduction equation can be written along with the surface energy balance as shown in equations 17 and 18.

$$\rho c_p \frac{\partial T}{\partial t} = \frac{1}{A} \frac{\partial}{\partial x} \left( kA \frac{\partial T}{\partial x} \right) \quad (17)$$

$$\dot{q}_{conv} + \alpha \dot{q}_{rad} - \dot{q}_{cond} - \epsilon \sigma T_w^4 = 0 \quad (18)$$

T = temperature

$T_w$  = the surface temperature

k = thermal conductivity

x = measured from TPS surface

$\rho$  = instantaneous material density

$C_p$  = material specific heat

$\dot{q}_{conv}$  = convective heat flux

$\dot{q}_{rad}$  = radiative heat flux

$\epsilon$  = material emissivity

$\alpha$  = material absorptivity

$\sigma$  = Stephan-Boltzman constant

This formulation neglects various forms of chemical fluxes entering the surface as well as the pyrolysis energy rate and the net energy absorbed due to pyrolysis gas movement through the material in the in-depth solution. The material decomposition, or the change in density, is computed explicitly as if it were a material property. The change in density as a function of temperature is computed using the aforementioned formulation of the Arrhenius equation [4]. Implicit discretization of the one-dimensional heat conduction equation was

performed using a finite-volume (also known as control-volume) technique.

## 6. TOOLSET INTEGRATION

Each of the disciplinary tools described above was “wrapped” and integrated into the commercially-available ModelCenter software, developed by Phoenix Integration. This integration environment allows direct linkage of input and output variables between the contributing analyses and expedites complete and synthesized conceptual analysis of a planetary entry mission. Variable values can be easily modified within the integration environment to enable rapid trades and sensitivity studies. If required, one of numerous optimization approaches may be incorporated. As shown in Figure 5, the PESST modules are set-up within the ModelCenter environment to run in a feed-forward fashion with a single feedback loop from the thermal response module to the trajectory simulation that iterates on heatshield mass.

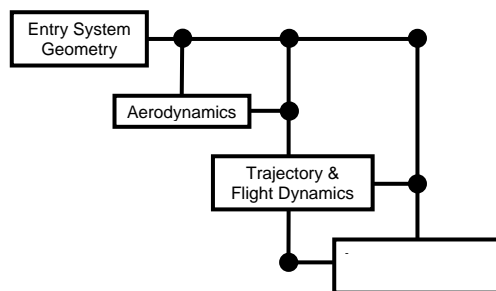


Fig. 5. PESST Design Structure Matrix

The validation exercise presented below provides a discussion of data flow between the disciplinary modules as well as the utility of this integrated environment.

## 7. VALIDATION

Throughout the development process, disciplinary tools were validated against analytical solutions, benchmark applications, and historical mission experience. Integrated tool performance was initially validated against Mars Pathfinder Flight (MPF) experience.

MPF utilized a  $70^\circ$  sphere-cone aeroshell design with a 0.6625m nose radius and a 2.65m maximum diameter for atmospheric entry. The aftbody cone angle was  $46.6^\circ$  and

the diameter of the backshell interference plate was 0.585m. These geometric parameters were input into PESST resulting in a volume of  $3.164\text{m}^3$ , a total surface area of  $13.88\text{m}^2$ , an aerodynamic reference data of  $5.515\text{m}^2$ , and a 3D vehicle model for visualization; all consistent with MPF values.

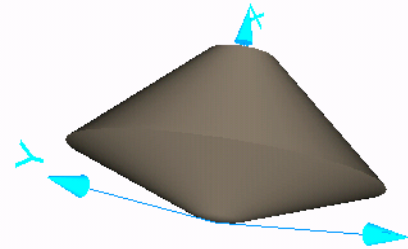


Fig. 6. PESST Model of MPF Aeroshell

Aerodynamic analysis of the generated surface mesh determined nominal drag coefficients of 1.649, 1.646, and 1.637 at  $0^\circ$ ,  $2^\circ$ , and  $5^\circ$  respectively. In comparison with representative values from the MPF aerodynamic database shown in Figure 7 and generated with the LAURA computational fluid dynamics code [7], the values generated within PESST have maximum errors of 4.6%, 3.9%, and 3.1% respectively over the hypersonic range. This error level is well within acceptable limits for PESST conceptual design applications.

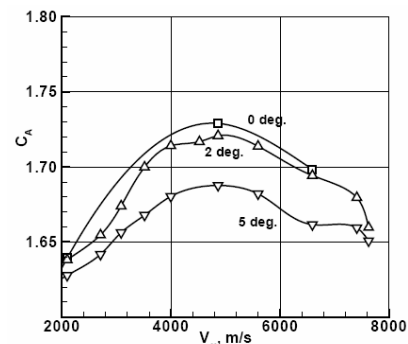


Fig. 7. MPF Axial Force Coefficients [7]

MPF entry occurred with a system mass of 585kg at a relative velocity of 7478.6 m/s, an altitude of 125km, and a  $-13.65^\circ$  flight path angle. The atmospheric interface latitude and longitude were  $22.63^\circ\text{N}$  and  $337.99^\circ\text{E}$ , and relative entry azimuth was  $253.67^\circ$  [8-10]. These entry conditions, along with event parameters specifying parachute deployment, heatshield jettison and backshell separation conditions as well as the geometric and



aerodynamic inputs linked within PESST, allow simulation of the atmospheric trajectory.

As shown in Figure 8, simulated time histories of velocity, flight path angle, and altitude compare well with MPF flight data. In addition, estimated heating rates, g-loading, and dynamic pressure compare equally well [8-10]. The simulation ends just prior to airbag inflation, less than 15km away from the actual landing site. This error is well within the expected dispersions and overall performance of the atmospheric trajectory simulation is satisfactory.

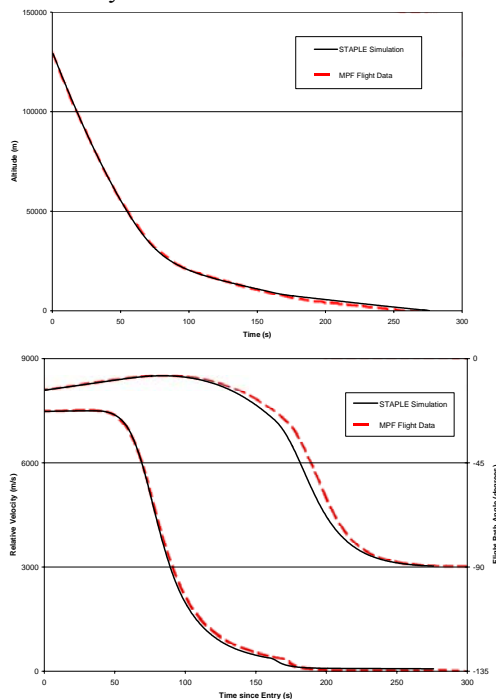


Fig. 8. MPF Trajectory Comparison

The MPF heatshield was constructed using SLA-561V with a stagnation point thickness of 1.91cm and an overall mass of 73.9kg. Iteration between the PESST trajectory simulation (to provide heating data) and the TPS sizing tool converged upon a TPS thickness of 2.39cm and a heatshield mass of 75.6kg with an error of 20% and 2.3% respectively from actual values. The PESST TPS thickness calculation includes a margin of 50% so that the “no-margin” thickness is 1.54cm, which compares remarkably well with the minimalist value of 1.52cm determined during MPF planning [11].

A screenshot of the tool, setup to model MPF, is shown in Figure 9 to illustrate the functionality and convenience of PESST. Note

that all key input and output variables are available for manipulation in the left console, a 3D vehicle model is present for visualization on the top right, and trajectory plots appear and update automatically as changes are made.

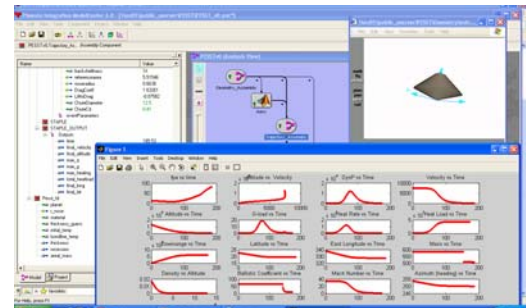


Fig. 9. Screenshot of PESST

## 8. SAMPLE APPLICATIONS

An initial version of PESST was utilized in support of the RASC Mars Human Precursor project led by Dr. Joel Levine at NASA LaRC to provide conceptual entry phase analysis for both Mars lander and Mars airplane missions.

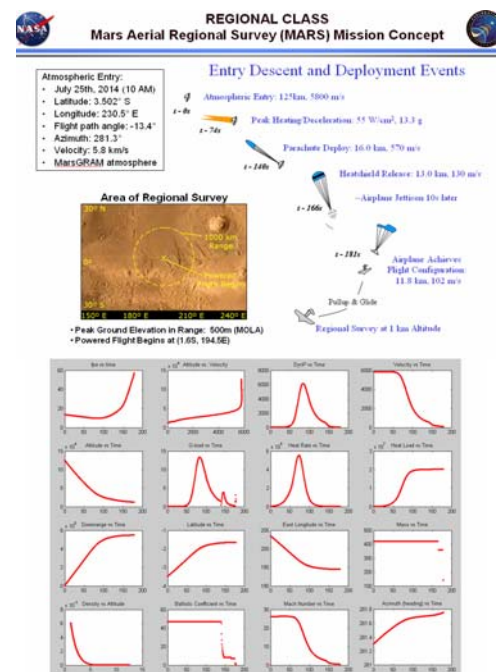


Fig. 10. Sample Application: Conceptual Entry Phase Analysis for a Mars Airplane Mission

In addition to modeling the entry event timeline and providing estimates of key entry phase parameters like maximum heat rate and maximum loads for nominal entry conditions as shown in Figure 10, sensitivity studies varying entry mass and flight path angle were

performed to estimate the maximum landed mass and volume for a MER heritage entry system. This analysis was performed by incorporating a mass estimation module that estimated landed mass and volume as a function of entry mass and volume based on historical experience. Results are shown in Figure 11 for a mission targeting a July 2012 landing at the site of Viking I. A MarsGRAM atmosphere was generated for this study and results are shown for entry flight path angles of  $-16.1^\circ$  and  $-12.0^\circ$ .

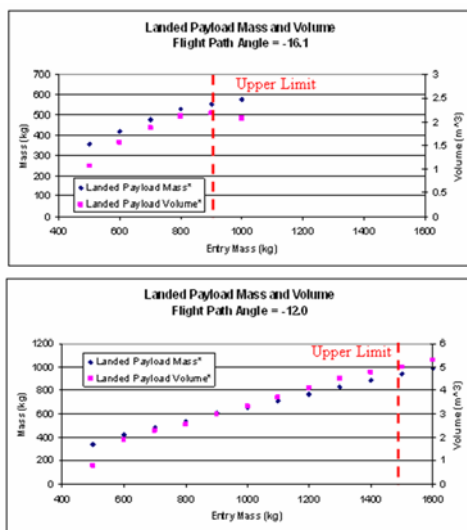


Fig. 11. Sample Application: Landed Mass and Volume Sensitivity Study

## 9. SUMMARY

An integrated framework for entry systems modeling and design has been developed to enable accelerated analysis of trades, allow for extensive design space exploration, and facilitate multidisciplinary design optimization. Comparison of PESST performance against Mars Pathfinder flight experience validates the tool's applicability to conceptual design studies and sensitivity analyses. While not presented in this paper, validation of the lifting, guided entry capability has also been performed against Aeroassist Flight Experiment (AFE) studies. PESST has also demonstrated utility in application to Mars Human Precursor mission design studies. This work has direct application to NASA's future robotic and human exploration systems and should lead to improvements in the conceptual modeling of planetary entry systems.

## 10. REFERENCES

- (1) Regan, F.J., Anandkrishnan, S.M., *Dynamics of Atmospheric Re-Entry*, AIAA Education Series, Washington, DC, 1993.
- (2) Vinh, N.X., Buseman, A., Culp, R.D., *Hypersonic and Planetary Entry Flight Mechanics*, The University of Michigan Press, Ann Arbor, MI, 1980. pp19-28.
- (3) Cerimele, C.J., Gamble, J.D., "A Simplified Guidance Algorithm for Lifting Aeroassist Orbital Transfer Vehicles", AIAA-85-0348
- (4) Anon, "User's Manual, Aerotherm Charring Material Thermal Response and Ablation Program", Acurex UM-87-13/ATD Acurex Corporation, Aerotherm Division, Mountain View, California, November, 1987
- (5) Sutton, K.S. and Graves, Jr., R.A., "A General Stagnation-Point Convective-Heating Equation for Arbitrary Gas Mixtures", NASA TR R-376, November 1971.
- (6) Tauber, M. E., Sutton, K., "Stagnation-Point Radiative Heating Relations for Earth and Mars Entries", *Journal of Spacecraft*, Vol. 28, No 1, 1991, pp.40-42.
- (7) Gnoffo, P.A., et al., "Prediction and Validation of Mars Pathfinder Hypersonic Aerodynamic Database", AIAA-98-2445
- (8) Milos, F.S., Chen, Y.K., "Mars Pathfinder Entry Temperature Data, Aerothermal Heating, and Heatshield Material Response," *Journal of Spacecraft and Rockets* vol. 36 no.3 pp380-391, 1999.
- (9) Spencer, D.A., et al. "Mars Pathfinder Entry, Descent, and Landing Reconstruction," *Journal of Spacecraft and Rockets* vol. 36 no. 3 pp357-366, 1999.
- (10) Desai, P.N., "Flight Reconstruction of the Mars Pathfinder Disk-Gap-Band Parachute Drag Coefficient," 17th AIAA Aerodynamic Decelerator Systems Technology Conference, Monterey, CA, May 2003.
- (11) Wilcockson, W.H., "Mars Pathfinder Heatshield Design and Flight Experience", *Journal of Spacecraft and Rockets*, vol. 39 no. 3, 1999.
- (12) Kipp, D.M., Braun, R.D., "Development of Trajectory Simulation Capabilities for the Planetary Entry Systems Synthesis Tool", URL: [www.ssd.gatech.edu](http://www.ssd.gatech.edu)
- (13) Dec, J.A., Braun, R.D., "Ablative Thermal Protection Sizing", (in preparation).